

Article

Fully Relaxed, Crack-Free AlGa_N with upto 50% Al Composition Grown on Porous GaN Pseudo-Substrate

Nirupam Hatui ^{1,*}, Henry Collins ¹, Emmanuel Kayede ¹, Shubhra S. Pasayat ^{1,2}, Weiyi Li ¹, Stacia Keller ¹ and Umesh K. Mishra ¹

¹ Department of Electrical and Computer Engineering, University of California, Santa Barbara, CA 93106, USA; henrycollins@ucsb.edu (H.C.); ekayede@ucsb.edu (E.K.); pasayat@wisc.edu (S.S.P.); weiyili@ece.ucsb.edu (W.L.); stacia@ece.ucsb.edu (S.K.); mishra@ece.ucsb.edu (U.K.M.)

² Department of Electrical and Computer Engineering, University of Wisconsin-Madison, Madison, WI 53706, USA

* Correspondence: nirupam@ucsb.edu

Abstract: Fully relaxed, crack free, smooth Al_xGa_{1-x}N layers with up to 50% Al composition were demonstrated on pseudo-substrates composed of dense arrays of 10 × 10 μm² compliant porous GaN-on-porous-GaN tiles. The AlGa_N layers were grown in steps for a total of 1.3 μm. The growth conditions necessary to demonstrate high quality films at higher Al compositions also suppressed any sidewall growth.

Keywords: AlGa_N; Porous GaN



Citation: Hatui, N.; Collins, H.; Kayede, E.; Pasayat, S.S.; Li, W.; Keller, S.; Mishra, U.K. Fully Relaxed, Crack-Free AlGa_N with upto 50% Al Composition Grown on Porous GaN Pseudo-Substrate. *Crystals* **2022**, *12*, 989. <https://doi.org/10.3390/cryst12070989>

Academic Editor: Paul J. Simmonds

Received: 20 June 2022

Accepted: 12 July 2022

Published: 16 July 2022

Publisher's Note: MDPI stays neutral with regard to jurisdictional claims in published maps and institutional affiliations.



Copyright: © 2022 by the authors. Licensee MDPI, Basel, Switzerland. This article is an open access article distributed under the terms and conditions of the Creative Commons Attribution (CC BY) license (<https://creativecommons.org/licenses/by/4.0/>).

1. Introduction

The wide bandgap tunability range of (Al,Ga)N from 3.4 eV for GaN to 6.1 eV for AlN allows for its use in deep ultraviolet (UV) light emitting diodes (LEDs) in fields such as medical disinfection, water purification, biochemical detection and UV curing [1–6]. In addition, high power UV laser diodes (LDs) are needed for solar-blind non-line-of-sight communications, UV spectroscopy, laser lithography, and optical data storage [7–11]. Recently, photonics integrated circuits have been of interest for developing self-powered UV photonics systems that can work sustainably and independently with a reduced size and power consumption for future on-chip optical communication [12–18]. For all these applications, high quality, large area AlGa_N substrates are needed. Bulk AlN substrates with a low dislocation density are the ideal candidate [19–24]; however, they are currently very expensive and only available in small sizes [25,26]. When AlGa_N is grown on foreign substrates such as silicon, sapphire, and silicon carbide, the lattice mismatch usually leads to films with a relatively high density of threading dislocations [27,28]. This is the main cause for non-radiative recombination, leading to the deterioration of the optical and electrical performance of AlGa_N UV optoelectronic devices [1,4,27]. When grown hetero-epitaxially on GaN, the lower lattice constant of AlGa_N leads to tensile strain and cracking with epilayers thicker than the critical thickness [29,30]. Using lateral overgrowth of buried cracks, relaxed Al_{0.2}Ga_{0.8}N layers on GaN templates were formed using plastic relaxation [31]. Lateral growth of AlGa_N on porous GaN or AlN base layers has also been pursued in an effort to reduce the dislocation density [32,33]. Several research groups have also attempted to use a sacrificial layer for flip chip UV LEDs [34].

Recently, 10 × 10 μm² patterned compliant porous GaN pseudo-substrates (PSs) were formed [35]. Due to its high surface-to-volume ratio, porous GaN exhibits reduced mechanical stiffness with increased porosity [36], similar to porous silicon [37], facilitating the elastic relaxation of InGa_N grown on porous GaN PSs [38,39]. On these patterned compliant pseudo-substrates, the growth of 1.3 μm thick crack free, elastically relaxed AlGa_N with a low Al composition was also demonstrated [40]. In this work, we performed

the deposition of fully relaxed AlGaN with an Al composition of up to 50% on similar GaN-on-porous-GaN PSs.

2. Materials and Methods

The layer structure used for porosification as the pseudo-substrate consisted of a 2.8 μm thick unintentionally doped (UID) GaN on c-plane sapphire followed by 800 nm Si doped GaN with a doping of $5 \times 10^{18} \text{ cm}^{-3}$ which was capped with 100 nm of UID GaN. The sample was patterned and dry etched with a 100 W BCl_3/Cl_2 etch, forming $10 \times 10 \mu\text{m}^2$ square tiles 2 μm apart and with an etch depth of 600 nm. The sidewalls of the tiles were aligned parallel to the orthogonal GaN $[\bar{1}100]$ and GaN $[11\bar{2}0]$ planes, respectively. The GaN:Si layers were then porosified with a doping selective electrochemical (EC) etch in 0.3 M oxalic acid with metal contact to the sample with anode and Pt wire acting as the cathode [41]. The current flowing through the sample caused a redox reaction resulting in GaN:Si etching, which formed GaN tiles with embedded porous GaN as depicted in the schematic in Figure 1a and as reported previously [35].

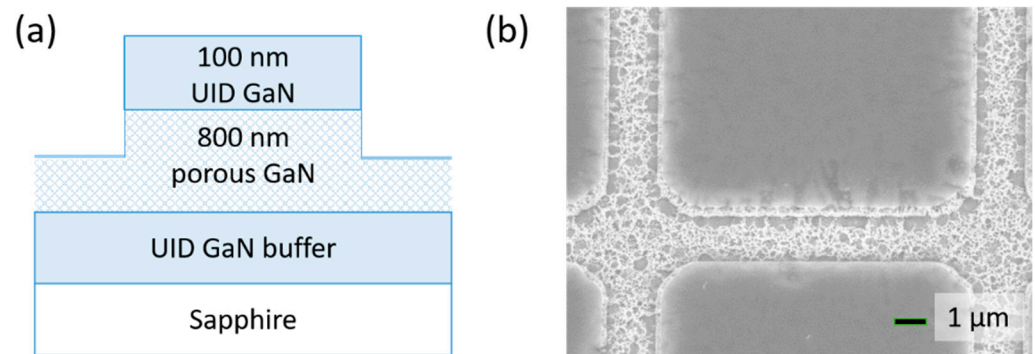


Figure 1. (a) Schematic structure of the GaN-on-porous-GaN pseudo-substrate. (b) Top view scanning electron microscopy image showing the tiles.

The epitaxial layers in this study were grown by metal organic vapor phase epitaxy (MOVPE) in a close coupled showerhead reactor using the precursors trimethylgallium (TMGa), trimethylaluminum (TMAI), and ammonia (NH_3) on the c-plane porous GaN pseudo-substrates at a pressure of 100 Torr. In our previous work, a total of 1.3 μm thick elastically relaxed AlGaN with $x_{\text{Al}} = 0.18$ was demonstrated using a growth temperature of 1080 $^\circ\text{C}$ and a mixture of hydrogen and nitrogen as the carrier gas [40]. To obtain good quality AlGaN films with a higher Al composition, the deposition temperature was increased to 1155 $^\circ\text{C}$ [42,43], and the NH_3 flow was decreased to 45 mmol/min from 178 mmol/min [40]. The molar flow of TMGa varied at 8.8–14.6 $\mu\text{mol}/\text{min}$ and TMAI was in the range of 0.98–2.4 $\mu\text{mol}/\text{min}$, respectively. However, growth under these conditions on the GaN-on-porous-GaN PSs resulted in the formation of circular islands on the sample surface (Figure 2a). While the higher growth temperature of 1155 $^\circ\text{C}$ was necessary to achieve high quality AlGaN at the targeted composition, it was not suitable for deposition on the GaN-on-porous-GaN PSs. In order to achieve smooth layers, a two-step process was implemented, where the initial 120–130 nm of AlGaN was grown at 1080 $^\circ\text{C}$ in a nitrogen ambient atmosphere, after which the temperature was increased to 1155 $^\circ\text{C}$ for the rest of the run and the subsequent AlGaN growth was performed in a hydrogen ambient atmosphere.

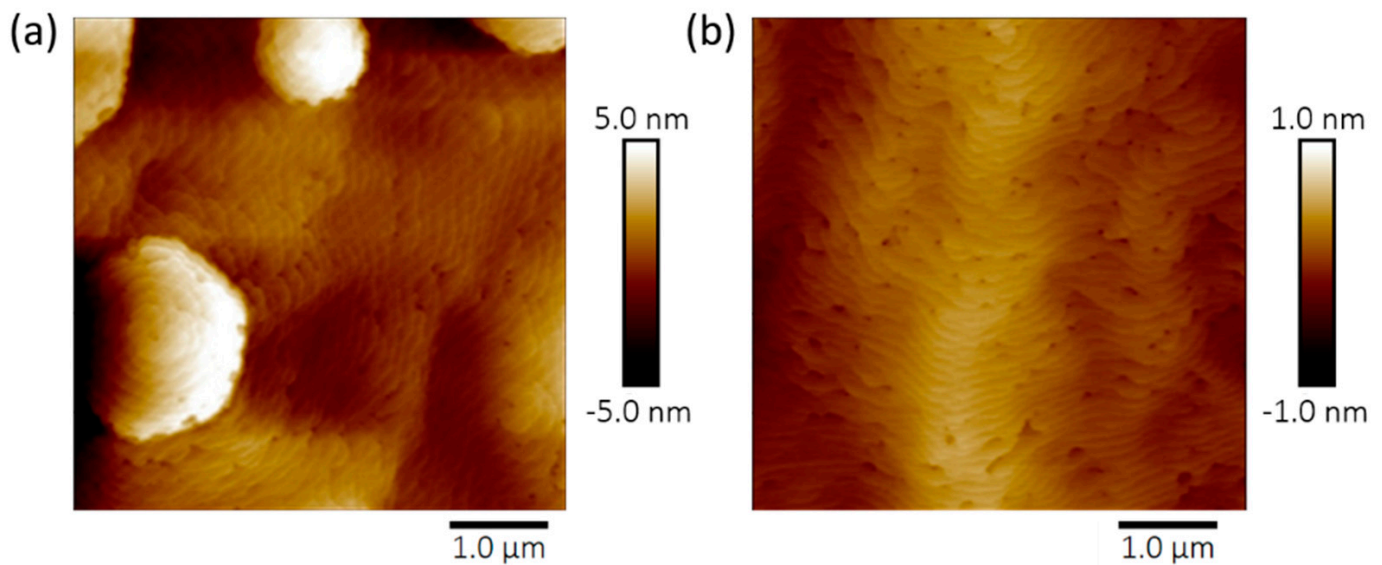


Figure 2. $5 \times 5 \mu\text{m}^2$ AFM images of AlGaIn grown at $1155 \text{ }^\circ\text{C}$ (a) on $10 \times 10 \mu\text{m}^2$ tiles of compliant pseudo-substrate; (b) on planar GaN, with image taken in the region in between cracks which developed due to strain.

The $1.3 \mu\text{m}$ thick AlGaIn layers were grown in steps, and before every regrowth the sample was solvent cleaned with acetone and isopropanol which was followed by a buffered HF dip and rinsing with deionized water to remove contaminants and the oxide layer introduced during characterization. The surface morphology was characterized using an optical microscope and atomic force microscope (AFM). High resolution x-ray diffraction (XRD) was used for rocking curve measurements to evaluate the film quality. Reciprocal space maps (RSMs) were taken using XRD around the GaN (1124) reflection. Composition and relaxation were determined from these RSMs using X-Pert Epitaxy software [44,45].

3. Experiment and Results

In the first experiment, the growth was initiated with 10 nm of GaN, which acted as a transition layer before introducing any strain in the structure, followed by 30 nm thick AlGaIn layers where the composition was increased in steps with target al. composition (x_{Al}) = 0.05, 0.09, 0.13 and 0.17 at $1080 \text{ }^\circ\text{C}$. Afterwards, the temperature was increased to $1155 \text{ }^\circ\text{C}$ and 30 nm each of AlGaIn with target x_{Al} = 0.21 and 0.25 was grown followed by 330 nm of AlGaIn with a target al. mole fraction of 0.30. The target x_{Al} was obtained from fully strained AlGaIn on GaN calibration samples. The sample was characterized and a further 400 nm of AlGaIn was regrown with adjusted TMAI and TMGa flows, so as to decrease x_{Al} and match the lattice constant to the existing epilayer. An additional regrowth was then performed for another 400 nm of AlGaIn to bring the total thickness of the AlGaIn layer to $1.3 \mu\text{m}$. The schematic of the full epitaxial layer structure grown on the pseudo-substrate is shown in Figure 3a.

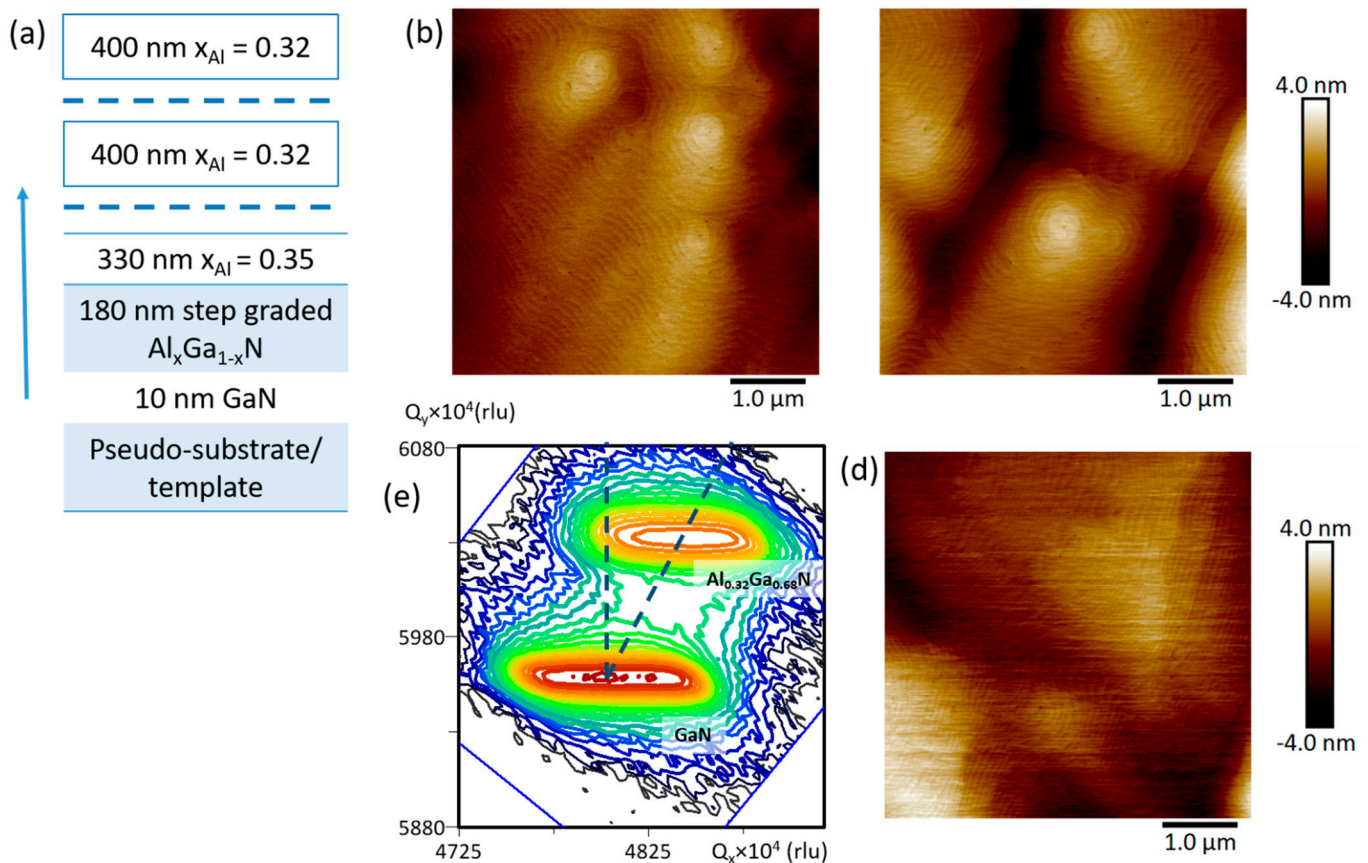


Figure 3. (a) Schematic of the first structure grown on porous GaN. The x_{Al} is obtained from RSM, and the dashed lines indicate regrowth interfaces. $5 \times 5 \mu\text{m}^2$ AFM height images of (b) initial ~ 500 nm AlGaIn; (c) after first regrowth (corresponding to $d_{\text{total}} \sim 900$ nm AlGaIn); (d) after second regrowth ($d_{\text{total}} \sim 1.3 \mu\text{m}$ AlGaIn) showing good surface morphology. (e) RSM obtained from XRD with the GaN and $1.3 \mu\text{m}$ AlGaIn peaks marked shows that $\text{Al}_{0.32}\text{Ga}_{0.68}\text{N}$ is fully relaxed. The vertical dashed line running up each scan from the GaN peak shows the strain line while the other dashed line is the fully relaxed line.

Evaluation of the initial ~ 500 nm thick AlGaIn structure revealed smooth, crack free layers (Figure 3b) with $x_{\text{Al}} = 0.35$ and a relaxation of $\sim 85\%$. The increase in measured Al composition over the targeted composition was expected due to the composition pulling effect [40,46–50]. The surface morphology remained smooth after the first and second regrowth (Figure 3c,d respectively). After the first regrowth (which brought the total thickness to ~ 900 nm), the AlGaIn peak corresponded to $x_{\text{Al}} = 0.32$ with $\sim 96\%$ relaxation. The final structure with $\sim 1.3 \mu\text{m}$ thick AlGaIn was fully relaxed and showed $x_{\text{Al}} = 0.32$ (Figure 3e).

With encouraging results having been obtained so far, a second porous PS sample was used to grow AlGaIn with a higher x_{Al} , following the structure depicted in the schematic in Figure 4a. A 10 nm GaN transition layer was again grown followed by a step-graded AlGaIn layer composed of 25 nm AlGaIn layers with target $x_{\text{Al}} = 0.05, 0.11, 0.17, 0.23,$ and 0.29 at 1080°C under nitrogen. As before, the temperature was then increased to 1155°C and 25 nm AlGaIn each with target $x_{\text{Al}} = 0.35,$ and 0.41 were grown followed by 325 nm of AlGaIn with a target x_{Al} of 0.47 in hydrogen. AFM images demonstrated a smooth surface morphology, and RSM showed an AlGaIn peak at $x_{\text{Al}} = 0.53$ with 89% relaxation (Figure 4b). After the solvent was clean and buffered in an HF dip, an additional 400 nm of AlGaIn was grown with a slightly reduced TMAI flow to lattice match with the already grown AlGaIn layer. The aluminum composition was 50% with 90% relaxation (Figure 4c). A further

400 nm regrowth increased the relaxation to 97% while maintaining the same aluminum content (Figure 4d,e).

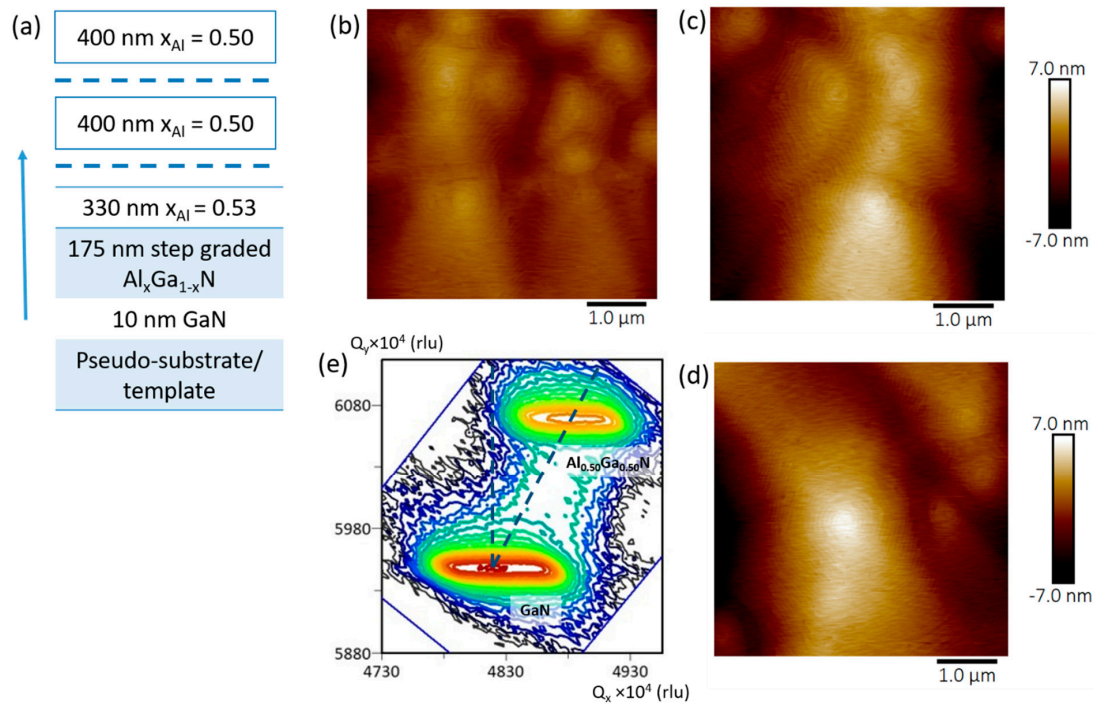


Figure 4. (a) Schematic of the second structure grown on porous GaN. The x_{Al} is obtained from RSM, and the dashed lines indicate regrowth interfaces. $5 \times 5 \mu\text{m}^2$ AFM height images of (b) initial ~ 500 nm AlGaN; (c) after first regrowth (corresponding to $d_{\text{total}} \sim 900$ nm AlGaN); (d) after second regrowth ($d_{\text{total}} \sim 1.3 \mu\text{m}$ AlGaN) showing good surface morphology. (e) RSM obtained from XRD with the GaN and $1.3 \mu\text{m}$ AlGaN peaks marked shows that $\text{Al}_{0.50}\text{Ga}_{0.50}\text{N}$ is fully relaxed. The vertical dashed line running up each scan from the GaN peak shows the strain line while the other dashed line is the fully relaxed line.

4. Discussion

Both the $1.3 \mu\text{m}$ thick AlGaN samples with $x_{\text{Al}} = 0.32$ and 0.50 showed no signs of cracking, and were fully relaxed. For the sample with $x_{\text{Al}} = 0.32$, AFM images showed a slight increase in roughness, presented as the root mean square (RMS) value in Figure 5 after the individual regrowth steps. The RMS roughness values increased slightly from 1.1 nm for the first ~ 500 nm stack to 1.4 nm after the first regrowth and decreased to 1.2 nm after the second regrowth, which is likely due to the AlGaN layer being already fully relaxed. The sample with $x_{\text{Al}} = 0.50$ showed an appreciable increase in roughness with the RMS value rising from 1.2 nm for the initial AlGaN stack to 2.7 nm after the first regrowth (with a total of ~ 900 nm AlGaN). The second regrowth stage showed no further increase in roughness. While the increase in surface roughness after the first regrowth step was unclear, the circumstance that the roughness did not further increase during the second regrowth suggests that the relaxed underlying AlGaN layer (after the first regrowth) prevented any stress-driven increase in surface roughness in this study, which is often observed when growing strained AlGaN layers.

Further XRD characterization to determine the ω -FWHM of the (002) and $(\bar{2}01)$ reflexes for the sample with $x_{\text{Al}} = 0.32$ showed 418 and 544 arc seconds, respectively, on par with good quality hetero-epitaxial growth [51,52]. Nevertheless, these values were higher than the underlying GaN layer for which ω -FWHM values of ~ 280 and 386 arc seconds for the (002) and $(\bar{2}01)$ reflexes, respectively, had been recorded. While the somewhat higher FWHM values could be the result of partial plastic relaxation, they could also be caused by local variations in relaxation and in the Al composition, between the edge and center

region of an individual tile, or tile to tile variations in the array. In addition, the elastic relaxation process could have led to tile tilt causing an increase in the ω -FWHM values.

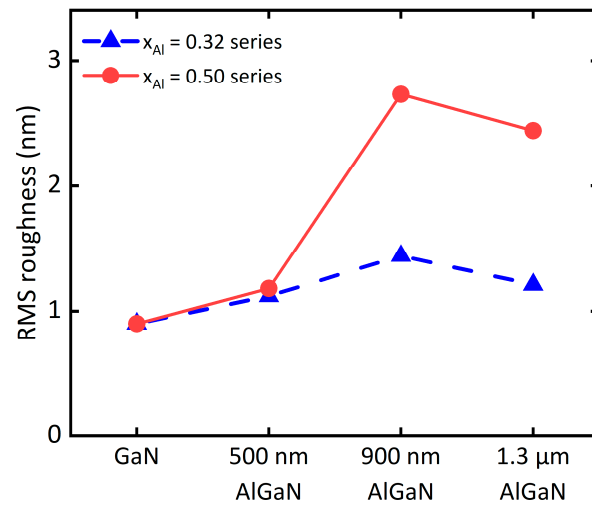


Figure 5. Graph showing the RMS surface roughness for the pseudo-substrate as well as after each AlGaIn growth for both $x_{Al} = 0.32$ and 0.50 samples. For the $x_{Al} = 0.32$ sample, the roughness remained generally flat, however, it increases after first regrowth for the $x_{Al} = 0.50$ sample.

For the sample with $x_{Al} = 0.50$, the (002) ω -FWHM amounted to 385 arc seconds, which was narrower than the value measured for the sample with $x_{Al} = 0.32$. In contrast, the (201) ω -FWHM increased to 677 arc seconds. This is a much more significant increase compared to the value of 386 arc seconds measured for the GaN base layer and the 544 arc seconds measured for the sample with $x_{Al} = 0.32$, which may be due to partial plastic relaxation under the formation of edge dislocations. Further investigations are currently underway to clarify the origin of the increase in FWHM, as well as to develop strategies to suppress it.

There was little evidence of growth on the tile sidewalls (Figure 6) which was observed previously when the AlGaIn layers were grown with a higher NH_3 flow of 178 mmol/min of NH_3 [38]. Lower NH_3 flow rates are known to suppress lateral growth [53] and could have been the cause for the lack of sidewall growth in this work. Further studies are planned to investigate this aspect, as sidewall growth may allow for tile coalescence to create large-area planar relaxed AlGaIn templates.

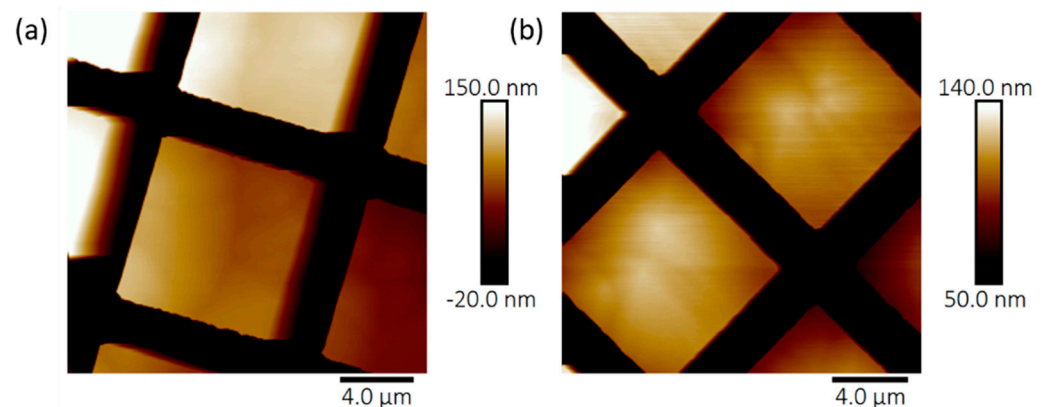


Figure 6. $20 \times 20 \mu\text{m}^2$ AFM height images of $1.3 \mu\text{m}$ AlGaIn grown on $10 \times 10 \mu\text{m}^2$ tiles of compliant pseudo-substrate; with (a) $x_{Al} = 0.32$ and (b) $x_{Al} = 0.50$. The $2 \mu\text{m}$ spacing between the tiles was preserved.

5. Conclusions

Fully relaxed, crack-free 1.3 μm thick AlGa_N layers with $x_{\text{Al}} = 0.32$ and 0.50 were formed on pseudo-substrates composed of $10 \times 10 \mu\text{m}^2$ compliant GaN-on-porous GaN tile arrays. The epilayers were smooth for $x_{\text{Al}} = 0.32$, while an increase in surface roughness and potential onset of partial plastic relaxation were observed for the sample with $x_{\text{Al}} = 0.50$. Further optimization of the step-graded layer and lateral growth can open up a pathway to obtain high quality, large area AlGa_N substrates as well as obtain fully relaxed AlGa_N with even higher values of x_{Al} .

Author Contributions: Investigation, N.H.; pseudo-substrate processing, H.C., S.S.P. and W.L.; atomic force microscopy, E.K., H.C. and N.H.; writing—original draft preparation, N.H.; writing—review and editing, S.K.; supervision, S.K. and U.K.M.; funding acquisition, U.K.M. All authors have read and agreed to the published version of the manuscript.

Funding: This work was supported by the Office of Naval Research (monitored by Dr. Paul Maki).

Data Availability Statement: The data that support the findings of this study are available within the article. More detailed findings of this study are available from the corresponding author upon reasonable request.

Conflicts of Interest: The authors declare no conflict of interest.

References

1. Kneissl, M.; Seong, T.Y.; Han, J.; Amano, H. The emergence and prospects of deep-ultraviolet light-emitting diode technologies. *Nat. Photon.* **2019**, *13*, 233–244. [[CrossRef](#)]
2. Moustakas, T.D.; Paiella, R. Optoelectronic device physics and technology of nitride semiconductors from the UV to the terahertz. *Rep. Prog. Phys.* **2017**, *80*, 106501. [[CrossRef](#)]
3. Ren, Z.; Yu, H.; Liu, Z.; Wang, D.; Xing, C.; Zhang, H.; Huang, C.; Long, S.; Sun, H. Band engineering of III-nitride-based deep-ultraviolet light-emitting diodes: A review. *J. Phys. D Appl. Phys.* **2019**, *53*, 073002. [[CrossRef](#)]
4. Li, D.; Jiang, K.; Sun, X.; Guo, C. AlGa_N photonics: Recent advances in materials and ultraviolet devices. *Adv. Optic. Photon.* **2018**, *10*, 43–110. [[CrossRef](#)]
5. Song, K.; Mohseni, M.; Taghipour, F. Application of ultraviolet light-emitting diodes (UV-LEDs) for water disinfection: A review. *Water Res.* **2016**, *94*, 341–349. [[CrossRef](#)]
6. Nagasawa, Y.; Hirano, A. A Review of AlGa_N-Based Deep-Ultraviolet Light-Emitting Diodes on Sapphire. *Appl. Sci.* **2018**, *8*, 1264. [[CrossRef](#)]
7. Sakai, T.; Kushimoto, M.; Zhang, Z.; Sugiyama, N.; Schowalter, L.J.; Honda, Y.; Sasaoka, C.; Amano, H. On-wafer fabrication of etched-mirror UV-C laser diodes with the ALD-deposited DBR. *Appl. Phys. Lett.* **2020**, *116*, 122101. [[CrossRef](#)]
8. Alkhazragi, O.; Hu, F.; Zou, P.; Ha, Y.; Kang, C.H.; Mao, Y.; Ng, T.K.; Chi, N.; Ooi, B.S. Gbit/s ultraviolet-C diffuse-line-of-sight communication based on probabilistically shaped DMT and diversity reception. *Optic Express* **2020**, *28*, 9111–9122. [[CrossRef](#)]
9. Vavoulas, A.; Sandalidis, H.G.; Chatzidiamentis, N.D.; Xu, Z.; Karagiannidis, G.K. A survey on ultraviolet C-band (UV-C) communications. *IEEE Commun. Surv. Tutor.* **2019**, *21*, 2111–2133. [[CrossRef](#)]
10. Zhang, Z.; Kushimoto, M.; Sakai, T.; Sugiyama, N.; Schowalter, L.J.; Sasaoka, C.; Amano, H. A 271.8 nm deep-ultraviolet laser diode for room temperature operation. *Appl. Phys. Expr.* **2019**, *12*, 124003. [[CrossRef](#)]
11. Drost, R.J.; Sadler, B.M. Survey of ultraviolet non-line-of-sight communications. *Semicond. Sci. Technol.* **2014**, *29*, 084006. [[CrossRef](#)]
12. Floyd, R.; Hussain, K.; Mamun, A.; Gaevski, M.; Simin, G.; Chandrashekhar, M.V.S.; Khan, A. An initial study of ultraviolet C optical losses for monolithically integrated AlGa_N heterojunction optoelectronic devices. *Phys. Status Solidi A* **2020**, *217*, 1900801. [[CrossRef](#)]
13. Floyd, R.; Hussain, K.; Mamun, A.; Gaevski, M.; Simin, G.; Chandrashekhar, M.V.S.; Khan, A. Photonics integrated circuits using Al_xGa_{1-x}N based UVC light-emitting diodes, photodetectors and waveguides. *Appl. Phys. Expr.* **2020**, *13*, 022003. [[CrossRef](#)]
14. Li, K.H.; Fu, W.Y.; Cheung, Y.F.; Wong, K.K.Y.; Wang, Y.; Lau, K.M.; Choi, H.W. Monolithically integrated InGa_N/Ga_N light-emitting diodes, photodetectors, and waveguides on Si substrate. *Optica* **2018**, *5*, 564–569. [[CrossRef](#)]
15. Li, K.H.; Cheung, Y.F.; Fu, W.Y.; Wong, K.K.Y.; Choi, H.W. Monolithic integration of Ga_N-on-Sapphire light-emitting diodes, photodetectors, and waveguides. *IEEE J. Sel. Top. Quant. Electron.* **2018**, *24*, 3801706. [[CrossRef](#)]
16. Lu, X.; Liu, C.; Jiang, H.; Zou, X.; Zhang, A.; Lau, K.M. Monolithic integration of enhancement mode vertical driving transistors on a standard InGa_N/Ga_N light emitting diode structure. *Appl. Phys. Lett.* **2016**, *109*, 053504. [[CrossRef](#)]
17. Liu, C.; Cai, Y.; Jiang, H.; Lau, K.M. Monolithic integration of III-nitride voltage controlled light emitters with dual-wavelength photodiodes by selective-area epitaxy. *Opt. Lett.* **2018**, *43*, 3401–3404. [[CrossRef](#)] [[PubMed](#)]
18. Chen, D.; Liu, Z.; Lu, X.; Wan, L.; Li, R.; Yang, Z.; Li, G. Efficiency improved by monolithic integration of HEMT with vertical-structure LEDs and Mg doping on dry etched Ga_N. *J. Mater. Chem. C* **2019**, *7*, 2823–2828. [[CrossRef](#)]

19. Liu, D.; Cho, S.J.; Park, J.; Seo, J.H.; Dalmau, R.; Zhao, D.; Kim, K.; Gong, J.; Kim, M.; Lee, I.K.; et al. 229 nm UV LEDs on aluminum nitride single crystal substrates using p-type silicon for increased hole injection. *Appl. Phys. Lett.* **2018**, *112*, 081101. [[CrossRef](#)]
20. Inoue, S.; Tamari, N.; Taniguchi, M. 150 mW deep-ultraviolet light-emitting diodes with large-area AlN nanophotonic light-extraction structure emitting at 265 nm. *Appl. Phys. Lett.* **2017**, *110*, 141106. [[CrossRef](#)]
21. Bryan, Z.; Bryan, I.; Xie, J.; Mita, S.; Sitar, Z.; Collazo, R. High internal quantum efficiency in AlGa_N multiple quantum wells grown on bulk AlN substrates. *Appl. Phys. Lett.* **2015**, *106*, 142107. [[CrossRef](#)]
22. Lochner, Z.; Kao, T.T.; Liu, Y.S.; Li, X.H.; Satter, M.M.; Shen, S.C.; Yoder, P.D.; Ryou, J.H.; Dupuis, R.D.; Wei, Y.; et al. Deep-ultraviolet lasing at 243 nm from photo-pumped AlGa_N/AlN heterostructure on AlN substrate. *Appl. Phys. Lett.* **2013**, *102*, 101110. [[CrossRef](#)]
23. Xie, J.; Mita, S.; Bryan, Z.; Guo, W.; Hussey, L.; Moody, B.; Schlessler, R.; Kirste, R.; Gerhold, M.; Collazo, R.; et al. Lasing and longitudinal cavity modes in photo-pumped deep ultraviolet AlGa_N heterostructures. *Appl. Phys. Lett.* **2013**, *102*, 171102. [[CrossRef](#)]
24. Martens, M.; Mehnke, F.; Kuhn, C.; Reich, C.; Küller, V.; Knauer, A.; Netzel, C.; Hartmann, C.; Wollweber, J.; Rass, J.; et al. Performance characteristics of UV-C AlGa_N-based lasers grown on sapphire and bulk AlN substrates. *IEEE Photon. Technol. Lett.* **2013**, *26*, 342–345. [[CrossRef](#)]
25. Bondokov, R.T.; Mueller, S.G.; Morgan, K.E.; Slack, G.A.; Schujman, S.; Wood, M.C.; Smart, J.A.; Schowalter, L.J. Large area AlN substrates for electronic applications: An industrial perspective. *J. Cryst. Growth* **2008**, *310*, 4020–4026. [[CrossRef](#)]
26. Sumathi, R.R.; Gille, P. Development and progress in bulk c-plane AlN single-crystalline template growth for large-area native seeds. *Jpn. J. Appl. Phys.* **2013**, *52*, 08JA02. [[CrossRef](#)]
27. Ban, K.; Yamamoto, J.; Takeda, K.; Ide, K.; Iwaya, M.; Takeuchi, T.; Kamiyama, S.; Akasaki, I.; Amano, H. Internal quantum efficiency of whole-composition-range AlGa_N multiquantum wells. *Appl. Phys. Express* **2011**, *4*, 052101. [[CrossRef](#)]
28. Reentilä, O.; Brunner, F.; Knauer, A.; Mogilatenko, A.; Neumann, W.; Protzmann, H.; Heuken, M.; Kneissl, M.; Weyers, M.; Tränkle, G. Effect of the AlN nucleation layer growth on AlN material quality. *J. Cryst. Growth* **2008**, *310*, 4932–4934. [[CrossRef](#)]
29. Ito, K.; Hiramatsu, K.; Amano, H.; Akasaki, I. Preparation of Al_xGa_{1-x}N/GaN heterostructure by MOVPE. *J. Cryst. Growth* **1990**, *104*, 533–538. [[CrossRef](#)]
30. Lee, S.R.; Koleske, D.D.; Cross, K.C.; Floro, J.A.; Waldrip, K.E.; Wise, A.T.; Mahajan, S. In situ measurements of the critical thickness for strain relaxation in AlGa_N/GaN heterostructures. *Appl. Phys. Lett.* **2004**, *85*, 6164. [[CrossRef](#)]
31. Bethoux, J.-M.; Vennéguès, P.; Natali, F.; Feltin, E.; Tottereau, O.; Nataf, G.; De Mierry, P.; Semond, F. Growth of high quality crack-free AlGa_N films on GaN templates using plastic relaxation through buried cracks. *J. Appl. Phys.* **2003**, *94*, 6499. [[CrossRef](#)]
32. Wang, T.; Bai, J.; Parbrook, P.J.; Cullis, A.G. Air-bridged lateral growth of an Al_{0.98}Ga_{0.02}N layer by introduction of porosity in an AlN buffer. *Appl. Phys. Lett.* **2005**, *87*, 151906. [[CrossRef](#)]
33. Qhalid Fareed, R.S.; Adivarahan, V.; Chen, C.Q.; Rai, S.; Kuokstis, E.; Yang, J.W.; Khan, M.A.; Caissie, J.; Molnar, R.J. Air-bridged lateral growth of crack-free Al_{0.24}Ga_{0.76}N on highly relaxed porous GaN. *Appl. Phys. Lett.* **2004**, *84*, 696. [[CrossRef](#)]
34. Bergmann, M.A.; Enslin, J.; Yapparov, R.; Hjort, F.; Wickman, B.; Mercinkevičius, S.; Wernicke, T.; Kneissl, M.; Haglund, Å. Electrochemical etching of AlGa_N for the realization of thin-film devices. *Appl. Phys. Lett.* **2019**, *115*, 182103. [[CrossRef](#)]
35. Pasayat, S.S.; Gupta, C.; Wong, M.S.; Wang, Y.; Nakamura, S.; DenBaars, S.P.; Keller, S.; Mishra, U.K. Growth of strain-relaxed InGa_N on micrometer-sized patterned compliant GaN pseudo-substrates. *Appl. Phys. Lett.* **2020**, *116*, 111101.
36. Huang, S.; Zhang, Y.; Leung, B.; Yuan, G.; Wang, G.; Jiang, H.; Fan, Y.; Sun, Q.; Wang, J.; Xu, K.; et al. Mechanical properties of nanoporous GaN and its application for separation and transfer of GaN thin films. *ACS Appl. Mater. Interfaces* **2013**, *5*, 11074. [[CrossRef](#)]
37. Fakir, S.; Montagne, A.; Rahmoun, K.; Iost, A.; Ziouche, K. Mechanical properties of porous silicon and oxidized porous silicon by nanoindentation technique. *Mater. Sci. Eng. A* **2018**, *711*, 470. [[CrossRef](#)]
38. Pasayat, S.S.; Wu, F.; Gupta, C.; DenBaars, S.P.; Nakamura, S.; Keller, S.; Mishra, U.K. Study of pore geometry and dislocations in porous GaN based pseudo-substrates using TEM. *IEEE J. Quant. Electron.* **2022**. [[CrossRef](#)]
39. Keller, S.; Pasayat, S.S.; Gupta, C.; DenBaars, S.P.; Nakamura, S.; Mishra, U.K. Patterned III-Nitrides on Porous GaN: Extending Elastic Relaxation from the Nano- to the Micrometer Scale. *Phys. Status Solidi RRL* **2021**, *15*, 2100234. [[CrossRef](#)]
40. Pasayat, S.S.; Hatui, N.; Li, W.; Gupta, C.; Nakamura, S.; DenBaars, S.P.; Keller, S.; Mishra, U.K. Method of growing elastically relaxed crack-free AlGa_N on GaN as substrates for ultra-wide bandgap devices using porous GaN. *Appl. Phys. Lett.* **2020**, *117*, 062102. [[CrossRef](#)]
41. Zhang, Y.; Ryu, S.W.; Yerino, C.; Leung, B.; Sun, Q.; Song, Q.; Cao, H.; Han, J.A. Conductivity-based selective etching for next generation GaN devices. *Phys. Status Solidi B* **2010**, *247*, 1713–1716. [[CrossRef](#)]
42. Hatui, N.; Rahman, A.A.; Maliakkal, C.B.; Bhattacharya, A. Direct MOVPE growth of semipolar (11 $\bar{2}$ 2) Al_xGa_{1-x}N across the alloy composition range. *J. Cryst. Growth* **2015**, *437*, 1–5. [[CrossRef](#)]
43. Tang, L.; Tang, B.; Zhang, H.; Yuan, Y. Review—Review of Research on AlGa_N MOCVD Growth. *ECS J. Solid State Sci. Technol.* **2020**, *9*, 024009. [[CrossRef](#)]
44. Pereira, S.; Correia, M.R.; Pereira, E.; O'Donnell, K.P.; Alves, E.; Sequeira, A.D.; Franco, N.; Watson, I.M.; Deatcher, C.J. Strain and composition distributions in wurtzite InGa_N/GaN layers extracted from X-ray reciprocal space mapping. *Appl. Phys. Lett.* **2002**, *80*, 3913. [[CrossRef](#)]

45. Wurm, C.; Collins, H.; Hatui, N.; Li, W.; Pasayat, S.; Hamwey, R.; Sun, K.; Sayed, I.; Khan, K.; Ahmadi, E.; et al. Demonstration of device-quality 60% relaxed $\text{In}_{0.2}\text{Ga}_{0.8}\text{N}$ on porous GaN pseudo-substrates grown by PAMBE. *J. Appl. Phys.* **2022**, *131*, 015701. [[CrossRef](#)]
46. Kobayashi, A.; Ohta, J.; Fujioka, H. Low temperature epitaxial growth of $\text{In}_{0.25}\text{Ga}_{0.75}\text{N}$ on lattice-matched ZnO by pulsed laser deposition. *J. Appl. Phys.* **2006**, *99*, 123513.
47. Even, A.; Laval, G.; Ledoux, O.; Ferret, P.; Sotta, D.; Guiot, E.; Levy, F.; Robin, I.C.; Dussaigne, A. Enhanced In incorporation in full InGaN heterostructure grown on relaxed InGaN pseudo-substrate. *Appl. Phys. Lett.* **2017**, *110*, 262103. [[CrossRef](#)]
48. Däubler, J.; Passow, T.; Aidam, R.; Köhler, K.; Kirste, L.; Kunzer, M.; Wagner, J. Long wavelength emitting GaInN quantum wells on metamorphic GaInN buffer layers with enlarged in-plane lattice parameter. *Appl. Phys. Lett.* **2014**, *105*, 111111. [[CrossRef](#)]
49. Chen, Z.; Pei, Y.; Newman, S.; Brown, D.; Chung, R.; Keller, S.; DenBaars, S.P.; Nakamura, S.; Mishra, U.K. Growth of AlGaN/GaN/AlGaN double heterojunction field-effect transistors and the observation of a compositional pulling effect. *Appl. Phys. Lett.* **2009**, *94*, 171117. [[CrossRef](#)]
50. Lund, C.; Hestroffer, K.; Hatui, N.; Nakamura, S.; DenBaars, S.P.; Mishra, U.K.; Keller, S. Digital growth of thick N-polar InGaN films on relaxed InGaN pseudosubstrates. *Appl. Phys. Express* **2017**, *10*, 111001. [[CrossRef](#)]
51. Zhang, Y.; Xing, Z.; Ma, Z.; Chen, Y.; Ding, G.; Xu, P.; Dong, C.; Chen, H.; Le, X. Threading dislocation density comparison between GaN grown on the patterned and conventional sapphire substrate by high resolution X-ray diffraction. *Sci. China Phys. Mech. Astron.* **2010**, *53*, 465–468. [[CrossRef](#)]
52. Zollner, C.J.; Almogbel, A.; Yao, Y.; SaifAddin, B.K.; Wu, F.; Iza, M.; DenBaars, S.P.; Speck, J.S.; Nakamura, S. Reduced dislocation density and residual tension in AlN grown on SiC by metalorganic chemical vapor deposition. *Appl. Phys. Lett.* **2019**, *115*, 161101. [[CrossRef](#)]
53. Kapolnek, D.; Keller, S.; Vetury, R.; Underwood, R.D.; Kozodoy, P.; DenBaars, S.P.; Mishra, U.K. Anisotropic epitaxial lateral growth in GaN selective area epitaxy. *Appl. Phys. Lett.* **1997**, *71*, 1204. [[CrossRef](#)]